Thermodynamic geometry of spin-one lattice models. II. Criticality and coexistence in the mean-field approximation

Riekshika Sanwari [*] and Anurag Sahay [†]
Department of Physics, National Institute of Technology Patna, Patna 800005, India

(Received 22 August 2021; accepted 24 February 2022; published 24 March 2022)

We continue our study of the thermodynamic geometry of the spin one model from A. Sahay and R. Sanwari, Phys. Rev. E **105**, 034134 (2022). by probing the state space geometry of the Blume-Emery-Griffiths model and the Blume-Capel model in their mean-field approximation. By accounting for the stochastic variables involved we construct from the thermodynamic state space two complementary two-dimensional geometries with curvatures R_m and R_q which are shown to encode correlations in the model's two order parameters, the magnetization m and the quadrupole moment q. The geometry is investigated in the zero as well as the nonzero magnetic field region. We find that the relevant scalar curvatures diverge to negative infinity along the critical lines with the correct scaling and amplitude. We then probe the geometry of phase coexistence and find that the relevant curvatures predict the coexistence curve remarkably well via their respective R-crossing diagrams. We also briefly comment on the effectiveness of the geometric correlation length compared to the commonly used Ginzburg-Landau correlation length vis-à-vis their scaling properties.

DOI: 10.1103/PhysRevE.105.034135

I. INTRODUCTION

In [1] (paper I) we had established the thermodynamic geometry of the one-dimensional spin one model starting from its exact free energy obtained via the transfer matrix calculation. Along with the full three-dimensional scalar curvature, two sectional curvatures R_m and R_q were also worked out which were found to correctly encode the correlation lengths for the spin-spin and the quadrupole-quadrupole correlations, respectively. We also extensively verified the "strong" Ruppeiner conjecture relating the inverse of the critical free energy to the scalar curvature,

$$R = \frac{\kappa}{\psi}, \tag{1}$$

which we termed *the Ruppeiner equation* (see [2] for a recent application). Using hyperscaling it is equivalent to the equality of R with the correlation volume ξ^d. Treated as a differential equation in the singular free energy the Ruppeiner equation could be solved to obtain the spin scaling function for the spin one model. Remarkably, the association of the scalar curvatures with the calculated correlation lengths often extended to regions far beyond criticality, thus corroborating what we termed the weak Ruppeiner conjecture. The latter relates the scalar curvature to the correlation volume over a range of parameter values reasonably far from criticality,

$$R \sim \xi^d. \tag{2}$$

In this work we extend our geometrical analysis to the mean-field approximation of the spin one model as obtained in [3]. The mean-field case immediately poses a challenge since, unlike the exactly solvable one-dimensional case, it does not have an in-built correlation length measure to compare with the scalar curvature. On the other hand, the Riemannian geometry arising out of the mean-field equations of state has an intrinsic curvature suggestive of a correlation volume of the physical system below which the assumptions of classical fluctuation theory break down. Geometry therefore ends up enriching the information content of the mean-field thermodynamics. In any case this is the claim we put to test here in the context of the mean-field Blume-Emery-Griffiths (BEG) model. Satisfyingly, our subsequent analysis substantiates this claim from several perspectives and also shines a light on the geometric correlation length as a somewhat better suited candidate to analyzing the scaling behavior in comparison to the commonly used Ginzburg-Landau correlation length. Also, it is more satisfying, if somewhat mystifying, that we can obtain the correlation length from the equations of state itself without needing to extend the thermodynamics to include space-dependent terms.

The outline of the work is as follows. In Sec. II we set up the mean-field Hamiltonian and describe its phase structure in some detail. While mainly a review, many of the formulas worked out in this section are integral to a subsequent geometric analysis of criticality and coexistence and, besides, are not readily available in the literature. We therefore solicit the patience of the reader. In Sec. III we carefully construct two thermodynamic geometries of the mean-field model suited to correlations in its two order parameters. In Sec. III A we outline our method of computing the scalar curvatures in the mean-field model. We then discuss the geometry near criticality in Sec. IV and near coexistence in Sec. V. In Sec. IV A we briefly comment on the scaling properties of the geometric correlation length as compared to the square gradient one

[*] riekshikas.phd19.ph@nitp.ac.in
[†] anuragsahay@nitp.ac.in

obtained via a Ginzburg-Landau extension of the mean-field Hamiltonian. In Secs. IV B, IV C, and IV D we discuss in turn the scaling of scalar curvatures near the zero-field critical line, the tricritical point, and finally near the wing critical line. In Secs. V A and V B we construct the geometric phase coexistence curves in zero-field and in non-zero-field regions, respectively, and compare with the standard phase coexistence curves. Finally, in Sec. VI we summarize our main results, underline the key message in our work, and point to some future directions.

II. THE MEAN-FIELD BEG MODEL AND ITS PHASE STRUCTURE

The BEG model has the most general reflection symmetric Hamiltonian for a classical spin one model with nearest-neighbor interactions. The Hamiltonian for the BEG model is written as [3]

$$\mathcal{H}_{\rm beg} = -J \sum_{\langle ij \rangle} S_i S_j - K \sum_{\langle ij \rangle} S_i^2 S_j^2 - H \sum_i S_i + D \sum_i S_i^2. \tag{3}$$

The Ising-like lattice spin variable S_i takes values $+1$, -1, and 0. The BEG Hamiltonian, its context, and the limiting case of the Blume-Capel (BC) model [4,5] were reviewed in paper I so we shall not repeat them here. We make a minor change in notation from paper I in that we no longer capitalize the order parameters for the spin and the quadrupole moment,

$$m = \langle S_i \rangle;\ q = \langle S_i^2 \rangle, \tag{4}$$

where m is the average magnetization per site and q is the average quadrupole moment per site.

The qualitative features of the phase structure are already captured in the mean-field approximation to the model, to which we turn now. The mean-field Hamiltonian can be written as

$$\mathcal{H}^{mf}_{\rm beg} = -\left(\frac{Jzm}{2} + H\right) \sum_i S_i - \left(\frac{Kzq}{2} - D\right) \sum_i S_i^2, \tag{5}$$

with z being the coordination number of the lattice. In the following we shall scale all the quantities by the factor Jz but shall continue to represent the scaled quantities by their unscaled symbols, so that we have $\mathcal{H}^{mf}_{\rm beg}/Jz \to \mathcal{H}^{mf}_{\rm beg}$, $H/Jz \to H$, $D/Jz \to D$, and for later reference, $\beta Jz \to \beta$. The ratio K/J will appear subsequently as ω.

In the mean-field Hamiltonian the effects of spin-spin and quadrupole-quadrupole interactions are approximated, respectively, by the effective H field and the effective D field. This results in a single-site Hamiltonian which is solvable, with the trade-off being that the magnetization m and the quadrupole moment q are to be obtained self-consistently by a minimization of the mean-field free energy which is obtainable from the partition function,

The self-consistent expressions for the magnetic moment and the quadrupole moment are obtained as

$$m = \frac{2 \sinh \beta(m+H)}{2 \cosh \beta(m+H) + e^{\beta D - \beta q \omega}} \tag{6}$$

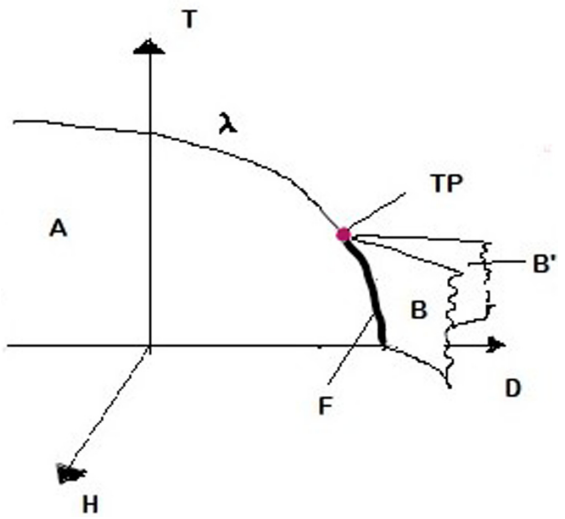

FIG. 1. Schematic diagram of the mean-field phase structure of the spin one model in the T-D-H space. Here the ratio K/J is small. Adapted from [6].

and

$$q = \frac{2 \cosh \beta(m+H)}{2 \cosh \beta(m+H) + e^{\beta D - \beta q \omega}}. \tag{7}$$

Making use of the above expressions the logarithm of the partition function can be written as

$$\psi = \log \mathcal{Z}_{mf} = \log \frac{q}{1-q} - \frac{1}{2}\beta(m^2 + q^2\,\omega), \tag{8}$$

and the free energy is

$$G = \frac{-\psi}{\beta}. \tag{9}$$

Of course, m and q in Eq. (8) still need to satisfy the self-consistent equations for equilibrium. Keeping in mind that in the BEG model it is the small values of ω that are physically relevant, we shall limit our investigations to such cases here. Nevertheless, we mention that the cases of larger ω (>1) have an interesting phase structure, some details of which may be found in [3].

In the superfluid phase where $m \neq 0$ the quadrupole moment q can be expressed in terms of m as

$$q = m \coth \beta(m+H), \tag{10}$$

and substituting this value for q in Eq. (6), m can be found self-consistently. In the normal phase, $m = 0$, q can be found from its transcendental equation. Equations (6) and (7) simplify considerably in the BC limit $\omega = 0$.

In Fig. 1 we present a mean-field phase diagram of the BC model [$\omega = 0$ with the Hamiltonian given by Eq. (3)]. The qualitative features remain the same for small values of ω [3,8]. Here **A** is a coexistence surface in the T-D plane where phases with positive and negative M coexist. In the limit $D \to -\infty$ only the $S = -1, 1$ states appear, and the system is mapped to a spin half Ising model. In the He^3-He^4 context it would mean the absence of any He^3 impurity. Also, there are symmetrically placed winglike coexistence surfaces **B** and **B**′ extending into the D-H plane for $D > D_{\rm tcr}$. The wings

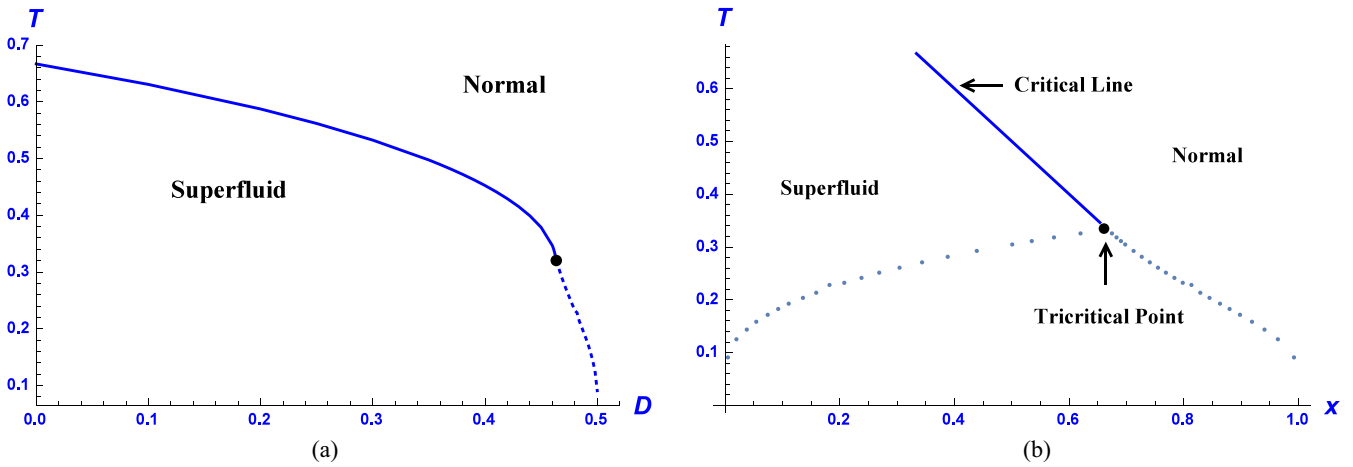

FIG. 2. (a) Plot of the zero-field critical and coexistence lines in the D-T plane for the BC model with $\omega = 0$. The black dot is the tricritical point at $D = 0.4621$ and $T = 1/3$, while the dotted line below is the coexistence curve and the smooth line above is the critical line. (b) The same phase structure in the x-T plane where $x = 1 - q$. The coexistence region is covered by the dotted curves. Both panels are adapted from [3].

act as coexistence surfaces for the paramagnetic states having different values of m and q. The coexistence surface **A** and the wings **B** and **B**′ each is bordered on the high-temperature side with critical lines which join together at the tricritical point **TP**. The line of intersection of the three coexistence surfaces is the triple line **F** which terminates at the tricritical point. At the tricritical point the values of the critical exponents β, δ, and α, where the symbols have the standard meaning as in [7], are different from their critical values, while the exponents γ and ν are the same [9].

In Fig. 2(a) we plot the zero-field critical line, tricritical point, and coexistence line in the D-T plane for the BC limit. As we have mentioned earlier, the phase structure remains the same for small values of ω in the BEG model. Referring readers to [3,10] for detailed derivations, we briefly outline here some mathematical relations pertaining to the phase structure. First, in the BC limit the zero-field expression for magnetization simplifies considerably,

$$m = \frac{2\sinh(\beta m)}{2\cosh(\beta m) + e^{\beta D}} \qquad (\text{BC}, H = 0), \tag{11}$$

and in the vicinity of the critical point the Landau expansion of the free energy gives

$$G = -\frac{\log\left(2e^{\beta(-D)} + 1\right)}{\beta} + \left(\frac{1}{2} - \frac{\beta}{e^{\beta D} + 2}\right) m^2 - \frac{[\beta^3(e^{\beta D} - 4)]}{12(e^{\beta D} + 2)^2} m^4 + \cdots . \tag{12}$$

The critical points are obtained via the condition $\partial^2 G/\partial m^2 = 0$ at $m = 0$ and the tricritical point via the additional condition that $\partial^4 G/\partial m^4 = 0$ at $m = 0$. This gives the equation of the zero-field critical line of the BC model as

$$D_{cr} = \frac{\log 2(\beta - 1)}{\beta} \qquad (\text{BC model}, H = 0), \tag{13}$$

and the tricritical point at

$$\left.\begin{aligned} \beta_{\text{tcr}} &= 3 \\ D_{\text{tcr}} &= \tfrac{\log 4}{3} = 0.4621 \end{aligned}\right\} \qquad (\text{BC tricritical point}).$$

Equation (13) should be used only for $\beta \leqslant 3$. For higher β values while the equation still gives critical values, it is for the metastable normal phase, which we shall not pursue here. It can also be verified that the zero-field coexistence line starting at the tricritical point touches $T = 0$ at $D = 0.5$. For higher values of D the superfluid state no longer remains globally stable at any temperature, though it remains locally stable. In other words, for $D > 0.5$ the normal state remains the preferred state for all temperatures down to zero. From Eq. (13) it may also be easily checked that for $D = 0$, which is just the three-state Ising model, the critical temperature is $\beta = 3/2$, and for $D \to -\infty$ in which limit the BC model tends to the two-state Ising model the critical temperature $\beta \to 1$ as expected. Also plotted in Fig. 2(b) is the phase diagram in the x-T plane which shows the critical line, the tricritical point, and the coexistence region. Here $x = 1 - q$ refers to the specific concentration of the He^3 phase.

We now briefly review the phase structure for the nonzero field for the BC case. Again, the phase structure is similar for the BEG case with small ω values. For nonzero field it is best to invert Eq. (6) for the magnetic moment and express the magnetic field H in terms of m,

$$H = \frac{1}{\beta}\log\left(\frac{m\,e^{\beta D} + \sqrt{m^2 e^{2\beta D} - 4m^2 + 4}}{2(1 - m)}\right) - m. \tag{14}$$

Interestingly, now this becomes a closed-form equilibrium relation. A typical isothermal plot of H vs m is shown in Fig. 3(a). The curve is analogous to the P-v isotherm in the van der Waals gas, and the phase transition point is similarly obtained by drawing an equal area Maxwell construction. On further lowering the temperature the isotherm will cross the critical point via an inflection given by $\partial^2 H/\partial\, m^2 = 0$, which

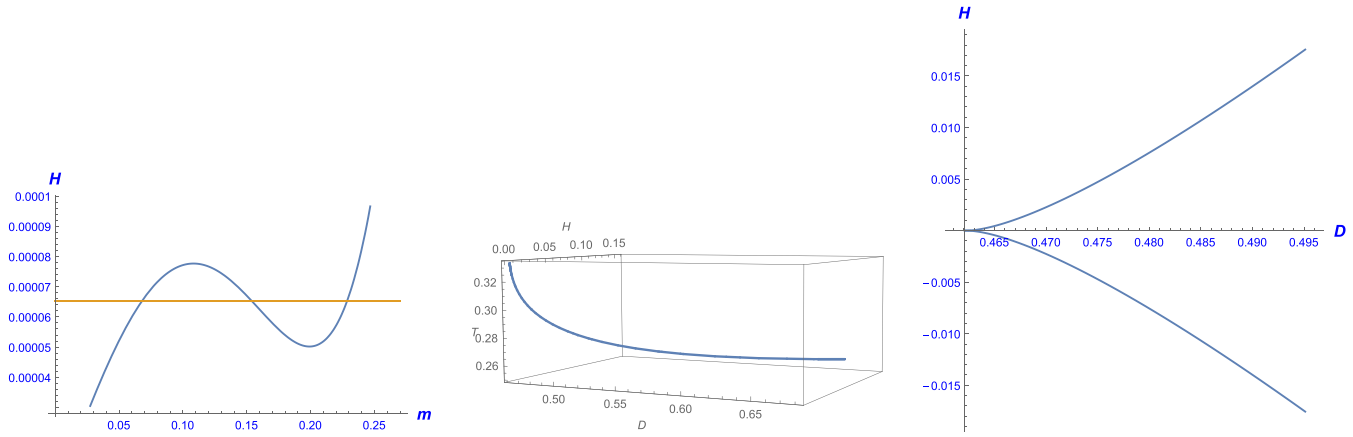

(a) (b) (c)

FIG. 3. (a) Isotherm in the $H-m$ plane at $D=0.4634$, $\beta=3.08$ shows phase coexistence via Maxwell construction at $H=0.000065$. (b) The non-zero-field critical line bordering from above the coexistence region or the "wing" in the D-H-T plane for the BC model with $\omega=0$. (c) The projection of the same critical line in the D-H plane. The leftmost point on the D axis is the tricritical point with $D=0.462$, $H=0$, and $T=1/3$.

in turn obtains the critical value of m in terms of β and D,

$$m_{cr}=\frac{\sqrt{e^{2\beta D}-16}(e^{2\beta D}-4)}{\sqrt{192e^{2\beta D}-48e^{4\beta D}+4e^{6\beta D}-256}}. \tag{15}$$

Further, on taking the second derivative of G in Eq. (9) with respect to m at $m=m_{cr}$ in Eq. (15) and then plugging in the value of critical H from Eq. (14) we can obtain simple relations between the parameters D, H, and β along the non-zero-field critical line [3],

$$\begin{aligned}H_{cr}&=\frac{1}{\beta}\log\left(\frac{\beta+\sqrt{(\beta-3)\beta}-2}{\sqrt{4-\beta}}\right)-\frac{1}{\beta}\sqrt{(\beta-3)\beta},\\ D_{cr}&=\frac{1}{2\beta}\log\left(\frac{16}{4-\beta}\right),\\ m_{cr}&=\frac{\sqrt{\beta-3}}{\sqrt{\beta}}.\end{aligned} \tag{16}$$

It can be easily ascertained from the equation above that along the non-zero-field critical line (or the "wing" critical line) β_{cr} ranges from three to four as D_{cr} ranges from $D_{\rm tcr}$ to infinity and H_{cr} ranges from zero to infinity. In Fig. 3(b) we plot the non-zero-field critical line in the D-H-T space. The critical line borders the coexistence "wing" under it, one each symmetrically placed in the positive and negative H direction. In Fig. 3(c) the symmetrically placed wings are projected upon the D-H plane.

Admittedly, we have left unexplored much of the parameter space, which in fact yields very rich phase structure. For example, at $\omega=3.1$ there are two more tricritical points symmetrically positioned on the critical boundaries of the wings **B** and **B**′ [3,8]. Moreover, negative values of the couplings J or K significantly change the phase behavior in the spin one model, [11,12]. We shall not pursue the cases of antiferromagnetic spin coupling or a repulsive biquadratic coupling in this work. While we believe the geometry of these cases well worth investigating, it will also be more subtle due to the presence of staggered spin and quadrupolar orders. We hope to return to these exciting cases in the future. In the limit $J=0$, which we call the Griffiths model, the BEG model exhibits phase coexistence as well as second-order transition in the quadrupolar order parameter [13]. In this limit the spin one model can be mapped onto the spin $\frac{1}{2}$ Ising model with a temperature-dependent magnetic field. Though we did explicitly work out the geometry of the Griffiths model in paper I, the geometry of its mean-field approximation turn out to be degenerate, as we shall see in the following.

III. CONSTRUCTING THE GEOMETRY OF THE MEAN-FIELD BEG MODEL

We start by accounting for the independent stochastic variables present in the full model and its mean-field approximation. To that end we first rewrite the full Hamiltonian (3) as a sum of stochastic variables

$$\mathcal{H}_{\rm beg}=\mathcal{F}_1+\mathcal{F}_2+\mathcal{F}_3, \tag{17}$$

where

$$\begin{aligned}\mathcal{F}_1&=-J\sum_{\langle ij\rangle}S_iS_j-K\sum_{\langle ij\rangle}S_i^2S_j^2,\\ \mathcal{F}_2&=-H\sum_i S_i,\\ \mathcal{F}_3&=D\sum_i S_i^2.\end{aligned} \tag{18}$$

The mean values of the random variables are related to the extensive thermodynamic quantities,

$$\langle\mathcal{F}_1\rangle=U;\ \langle\mathcal{F}_2\rangle=-H\,M;\ \langle\mathcal{F}_3\rangle=D\,Q, \tag{19}$$

where M is the mean total magnetization, Q is the mean total quadrupole moment, and U is the average "internal" energy of the BEG system, arising out of mutual interactions between spins and quadrupole moments at different lattice sites. The three random variables are independent (though correlated), thus implying that in the parameter space there are three *independent* directions of equilibrium fluctuations.

Except for the one-dimensional spin one model [6] and a few special two-dimensional cases it is not possible to compute the partition function analytically. On the other hand the mean-field partition function is easily computed, and, as the Monte Carlo simulations bear out, its phase structure is qualitatively correct, [14]. Therefore it is worthwhile exploring the geometry of the mean-field model. Unlike the full Hamiltonian the mean-field model loses all direct information about the internal correlations and retains only the average effect of interactions. In particular, the random variable $\mathcal{F}_1$ of Eq. (18) is no more independent, thus bringing down the number of stochastic variables to two. We rewrite (scaled) Eq. (5) for the mean-field Hamiltonian to delineate the three random variables,

$$\begin{aligned}\mathcal{H}^{mf}_{\rm beg} &= -\left(\frac{m}{2}\sum_i S_i + \frac{\omega\, q}{2}\sum_i S_i^2\right)\\ &\quad - H\sum_i S_i + D\sum_i S_i^2,\\ &= \mathcal{F}_1^{mf} + \mathcal{F}_2 + \mathcal{F}_3. \end{aligned} \tag{20}$$

With its equilibrium fluctuations governed by the fluctuations and correlations in $\mathcal{F}_2$ and $\mathcal{F}_3$ the internal energy random variable $\mathcal{F}_1^{mf}$ carries no additional information about the underlying system, unlike its full BEG counterpart in Eq. (18).

We emphasize a crucial point here, namely, that even as the parameter space of the mean-field BEG model is three-dimensional with independent T, H, and D directions, at any point in its Riemannian thermodynamic manifold the tangent space of fluctuating directions is only two-dimensional. We believe that it is generally true that the number of independent stochastic variables in any mean-field approximation of any model is at least one less.

This is similar to the case of the two-state Ising model, to which we digress for a bit, where the mean-field Hamiltonian has only one independent random variable, [15,16], while the full Hamiltonian has two. This can be seen by recalling the equation of the Ising model Hamiltonian,

$$\mathcal{H}_{\rm ising} = -J\sum_{\langle ij\rangle} S_i S_j - H\sum_i S_i, \tag{21}$$

and that of its mean-field approximation after rescaling by Jz as

$$\mathcal{H}^{mf}_{\rm ising} = -\left(H + \frac{m}{2}\right)\sum_i S_i. \tag{22}$$

Thus, while the parameter space remains two-dimensional with T and H as independent directions, the mean-field approximation in Eq. (22) has the only independent stochastic variable resulting in a one-dimensional state space geometry. This is also be seen by examining the expression for the mean-field entropy S of the two-state Ising model,[1]

$$S = \log\frac{2}{\sqrt{1-m^2}} - m\tanh^{-1} m, \tag{23}$$

from which it is clear that the entropy depends only on one extensive variable, thus rendering the geometry degenerate.

With two independent random variables the mean-field BEG model in Eq. (5) or (20) permits a nontrivial state space Riemannian geometry. As stated earlier, at any given point in the three-dimensional parameter space of the mean-field model there are only two independent directions of equilibrium fluctuations. This means that if we take an arbitrary two-dimensional equilibrium hypersurface in the three-dimensional parameter space and in principle constrain the system to undergo spontaneous fluctuations only on the given hypersurface, then the thermodynamic metric defined on it will set up a two-dimensional Riemannian manifold. The thermodynamic metric on the hypersurface is straightforwardly obtained by taking the derivatives of the entropy (or the free energy) only along directions tangent to the hypersurface.[2] In a sense, each hypersurface carries its own two-dimensional Riemannian geometry, since, unlike the case in paper I, there is no ambient three-dimensional metric from which the projection metrics on these hypersurfaces could be induced. Apart from this crucial difference with the geometry of the 1D spin one model we shall construct the relevant hypersurface geometries for the mean-field case in an exactly analogous manner.

Following paper I here too we shall pursue the intrinsic thermodynamic geometries on the constant H surface and the constant D surface. Similarly, we find it easier to work with the Massieu functions, which we could express from Eq. (8) either as $\psi_D(\beta,\nu)$ with D constant or as $\psi_H(\beta,\mu)$ with H constant. The thermodynamic laws relevant to the first and the second geometries are

$$d\psi_D = -(U + QD)\, d\beta - M\, d\nu, \tag{24}$$

$$d\psi_H = -(U - HM)\, d\beta + D\, d\mu. \tag{25}$$

In both cases the Massieu function is the same, but the different arguments are emphasized here since the Riemannian metrics will be built out of the double derivatives in the arguments.

Following paper I it can be expected that in the first case the Riemannian geometry would be more sensitive to the fluctuations in the magnetic moment as compared to the quadrupole moment, while in the second case the opposite would be true. Accordingly, we shall sometimes refer to the first geometry which restricts fluctuations to the constant D plane in the T-H-D parameter space as the m geometry, with the metric and scalar curvature on the surface termed the m metric and R_m, and the second one which limits fluctuations to the constant H plane the q geometry with its associated q metric and R_q.

It is immediately obvious from Eq. (20) that the q geometry becomes degenerate in the normal phase with $m = H = 0$. This is because with the q geometry fluctuations restricted to the $H = 0$ plane all the coefficients of the stochastic variable

[1] Indeed, the entropy label S is not to be confused with the spin label S_i.

[2] Indeed, such a construction would break down on hypersurfaces where one of the directions of independent fluctuations happens to be orthogonal to the surface.

$\sum_i S_i$, including the variable itself, vanish leaving only a single random variable $\sum_i S_i^2$ free to fluctuate in the plane. On the other hand the m geometry, which is defined on the D plane, continues to remain nondegenerate in the normal phase since any fluctuation orthogonal to the H plane amounts to a nonzero m as well as H, so that both stochastic variables need to be retained. A somewhat limiting consequence of this is that in the normal phase there is only the curvature R_m to guide us. However, everywhere else in the parameter space both curvatures inform the underlying correlations in the two order parameters. We mention here that possibly there could be a way to resurrect the q geometry in the normal phase by adding a lattice-dependent energy term to the Hamiltonian in Eq. (20). We shall not be pursuing this line here but refer to [15] and [16], where such an approach was used in the context of the mean-field Ising model.

We also note that the geometry of the isotropic mean-field BEG model, obtained by setting $H = D = 0$ in Eq. (20), was worked out in [17] using an unconventional 2D metric different from ours in that it was obtained by taking double derivatives of the Helmholtz free energy with respect to m and q but not the temperature. While it is not *a priori* clear how the resulting line element would relate to the probability of fluctuation between nearby equilibrium states, the "mq" scalar curvature obtained from the metric was nevertheless shown to have the right scaling behavior, and its sign changes were also shown to be closely aligned to the ferromagnetic and paramagnetic phases. In this paper, as in paper I, the metrics always follow from the first and second law variations of potentials as explained in [18].

A. Calculating the state space scalar curvatures

Finally, we give an outline of our calculations for the metric and the associated curvature in the mean-field case. Unlike the one-dimensional case of paper I the mean-field free energy depends directly as well as indirectly on the parameters β, μ, and ν via its dependence on m and q, which are themselves implicit functions of the parameters through their self-consistent Eqs. (6) and (7). As a result any derivative of the free energy will necessarily involve the derivatives of m or q with respect to β, ν, or μ, where the set of free parameters depends on whether the curvature R_q or R_m is being calculated. For example, in the calculation of R_m the starting point is the m metric, which is obtained by taking the Hessian of ψ in Eq. (9) by considering it as a function of β and ν with D fixed, Eq. (24),

$$\psi_D(\beta,\nu) = \log\frac{q_D(\beta,\nu)}{1-q_D(\beta,\nu)} - \frac{1}{2}\beta[m_D(\beta,\nu)^2 + q_D(\beta,\nu)^2\,\omega]. \quad (26)$$

Now any derivative of ψ_D with respect to β or ν will involve derivatives of $m(\beta,\nu)$ or $q(\beta,\nu)$ and to that end we first rewrite Eqs. (6) and (7) to reflect this,

$$m_D(\beta,\nu) = \frac{2\sinh[\beta\, m_D(\beta,\nu)+\nu]}{\mathcal{D}} \quad (27)$$

and

$$q_D(\beta,\nu) = \frac{2\cosh[\beta\, m_D(\beta,\nu)+\nu]}{\mathcal{D}}, \quad (28)$$

where $\mathcal{D}$ equals

$$\cosh[\beta\, m_D(\beta,\nu)+\nu] + \exp[\beta\, D - \beta\,\omega\, q_D(\beta,\nu)].$$

After differentiating both sides of Eqs. (27) and (28) we can solve them simultaneously to obtain the first-order derivatives back in terms of m and q. The expressions are too large to report here. Any higher order derivative can therefore consistently be expressed in terms of m and q. Finally, the curvature R_m is obtained in terms of the parameters β, H, D, and in terms of m and q. Of course, the equilibrium values of the latter will depend on the parameters via the implicit relations in Eqs. (6) and (7).

Similarly, in order to obtain the geometry on hypersurfaces parametrized by H we rewrite the magnetization and quadrupole moment as functions of β and μ:

$$m_H(\beta,\mu) = \frac{2\sinh\beta[m_H(\beta,\mu)+H]}{\mathcal{D}} \quad (29)$$

and

$$q_H(\beta,\mu) = \frac{2\cosh\beta[m_H(\beta,\mu)+H]}{\mathcal{D}}, \quad (30)$$

where now $\mathcal{D}$ is rewritten as

$$\cosh\beta[m_H(\beta,\mu)+H] + \exp[\mu - \beta\,\omega\, q_H(\beta,\mu)].$$

The starting point for geometric calculations on the H surface is the free energy, Eq. (9), recast as a function of β and μ and parametrized by H,

$$\psi_H(\beta,\mu) = \log\frac{q_H(\beta,\mu)}{1-q_H(\beta,\mu)} - \frac{1}{2}\beta[m_H(\beta,\mu)^2 + q_H(\beta,\mu)^2\,\omega]. \quad (31)$$

In an analogous manner the derivatives with respect to β and μ can be solved for, finally leading to an expression for the curvature R_q.

IV. GEOMETRY OF CRITICALITY

We now probe the scaling behavior of the state space scalar curvature in light of the Ruppeiner equation, which relates the curvature to the inverse of the critical free energy.

With its three-dimensional parameter space the singular free energy of the BEG model can depend on up to three independent scaling fields obtained from a linear combination of deviations of the magnetic field H, the anisotropy field D, and the temperature T from their respective critical values. For the full BEG Hamiltonian of Eq. (3) this is indeed the case as is worked out thoroughly in [24], especially near the tricritical point. We are unable to ascertain if this will hold out in the mean-field context, given that the number of random variables here is reduced to two. In any case since the focus of our investigation is the geometry in either the H plane or the D plane we shall restrict the scaling analysis to these planes only, so that the critical free energy here shall have only two scaling fields.

Following [18] we first briefly summarize the context for obtaining the asymptotic form of scalar curvature. The scaling form of the singular free energy density can be expressed in

terms of the scaling fields $t = (\beta_c - \beta)/\beta_c$ and the ordering field h as

$$\omega(t, h) = n_1 t^{2-\alpha} Y(n_2 h t^{-\widetilde{\beta}\delta}), \tag{32}$$

where the universal critical exponents α, $\widetilde{\beta}$, and δ have their usual meanings as critical exponents, while the constants n_1 and n_2 are nonuniversal and system dependent.[3] $Y(z)$ is the spin scaling function which depends on h and t in a single argument combination $z = ht^{-\widetilde{\beta}\delta}$. Using the scaling form of free energy from Eq. (32) in the evaluation of R and putting it back into the Ruppeiner equation in Eq. (1), one obtains a third-order differential equation for the function $Y(z)$, which in turn leads to the scaling form of R, [18],

$$R = \frac{\widetilde{\beta}(\widetilde{\beta}\delta - 1)(\delta - 1)k_B T_c}{(2-\alpha)(1-\alpha)Y(0)} t^{\alpha-2}. \tag{33}$$

On the other hand the constant field-specific heat C_h can be evaluated directly from Eq. (32), and its leading singular part in zero field is

$$C_h = -\frac{(2-\alpha)(1-\alpha)Y(0)t^{-\alpha}}{T_c}. \tag{34}$$

The product of the scaling forms of R and C_h from Eqs. (33) and (34) given as

$$RC_h t^2 = -\widetilde{\beta}(\delta - 1)(\widetilde{\beta}\delta - 1)k_B \tag{35}$$

is consistent with the conjectured correspondence of R with the correlation volume ξ^d (and hence with the inverse free energy via hyperscaling). This follows from a well-known prediction of two-scale-factor universality according to which the product similar to the one in Eq. (35), with R replaced by the correlation volume ξ^d, is shown to be equal to a constant which depends only on the universality class [18,20].

In the following we shall present our main results for the geometry near the zero-field critical line, tricritical point, and wing critical line. But, first, we pause briefly to make some general comments in favor of the geometric correlation length obtained via the state space scalar curvature.

A. Geometric vs the Ginzburg-Landau correlation length: A divertissement

It shall be the main task of this paper to make a case that the curvatures R_m and R_q faithfully represent, to a large extent, the correlation lengths in the order parameters m and q, respectively. We repeat that unlike the one-dimensional case where the correlation length is exactly calculable via the transfer matrix and hence easily comparable to its geometric counterpart, there is no direct way to determine correlation length in a mean-field setup since we have already averaged out the effect of spin-spin interactions here. The standard way of getting around this limitation is to add a square gradient term as a first correction to the mean-field Hamiltonian, assuming a slow spatial variation in the order parameter [7].

[3]To avoid confusion we shall refer to the "critical exponent β" by the symbol $\widetilde{\beta}$ while reserving the symbol β for the inverse temperature.

TABLE I. Table comparing in different dimensions the Ising critical exponent ν obtained via the standard renormalization group calculations (labeled "true"), the ones obtained via thermodynamic geometry (labeled "geometric"), and the mean-field value.

Dimension	True ν	Geometric ν	Mean field ν
2	1	1	0.5
3	0.630	0.667	0.5
4	0.5	0.5	0.5

From the resulting Ginzburg-Landau (GL) Hamiltonian we can obtain a correlation length which scales at $h = 0$ as

$$\xi_{mf} \sim t^{-1/2} \quad \text{(G-L mean field)} \tag{36}$$

irrespective of the universality class to which the critical point belongs. Thus the exponent $\nu = 1/2$, and the upper critical dimension for ordinary critical points in $d = 4$.

We recall that the geometric method of estimating the scalar curvature is distinctly different. The curvature length scale in the state space manifold is the one *beyond* which the local flatness approximation does not hold, and this translates in the thermodynamic system to the physical volume scale *below* which the local correlation effects become strong enough for the assumptions of classical thermodynamic fluctuation theory to become invalid [18]. In other words, it is the correlation volume. Significantly, scalar curvature proves to be an *in-built*, invariant measure of the correlation length obtained using information already available from thermodynamics.

In this work for the BEG model, as for the van der Waals case earlier, [18,21], the universality class remains of the Ising type with well-known critical exponents obtained theoretically. As we shall also see in the following the state space scalar curvature is always found to have the same scaling near the critical point for models, which belong to the Ising class,

$$R \sim t^{-2} \quad \text{(Ising class)}. \tag{37}$$

Given that the state space scalar curvature scales as the correlation volume ξ^d we can obtain the exponent ν from geometry in a straightforward manner. In Table I we compare the Ising, the geometric, and the mean-field critical exponent ν for different dimensions

While all this should certainly not be taken as a suggestion of any superiority of the geometric correlation length over the square gradient one (the latter has a very well-founded basis and well-established usefulness), it certainly does help substantiate the Ruppeiner conjecture relating the state space scalar curvature to the correlation length, especially near criticality. Additionally, we hope it could also inform the RG calculations [22], and, coupled with the fact that the geometric curvature is straightforward to calculate, it could also help speed up such calculations. Significantly, as was pointed out in [23] in the context of simple fluids, and in paper I for the one-dimensional spin one model, the association of R with the correlation length might go far beyond the neighborhood of the critical region. In fact, we shall have ample opportunity in the following to confirm that, consistent with Widom's arguments equating the correlation lengths across the interface,

the scalar curvatures in the coexisting phases reasonably agree with each other in places far enough from criticality.

In the following sections we investigate, in turn, the thermodynamic geometry near the critical points and near the coexistence points, both in the zero-field and in the nonzero magnetic field.

B. Geometry near the zero-field critical line λ

1. The m geometry

We first discuss the BC case ($\omega = 0$), for which we are able to obtain relatively tractable algebraic expressions. In order to obtain a scaling expression of the scalar curvature R_m we first find its value in the normal phase with $m = 0$,

$$R_m = -\frac{\mathcal{N}}{2D^2(-2\beta + e^{\beta D} + 2)^2}, \tag{38}$$

where

$$\mathcal{N} = (1 + 2e^{-\beta D})(De^{\beta D} - 2) \times \{D[-2\beta + (\beta + 1)e^{\beta D} + 2] - e^{\beta D} - 2\}.$$

We then expand R_m^{-1} in powers of the small parameter $t = (\beta_c - \beta)/\beta_c$ in the neighborhood of the critical line given by Eq. (13). The dominant term in the expansion is

$$R_m^{-1} = -2(\beta_c - 1)D_c^2 t^2 + O(t^3) \tag{39}$$

This also shows that R_m is always negative near criticality since $\beta_c > 1$ for any finite D as shown in Eq. (13).

On the other hand, the zero-field specific heat C_h in the normal phase is obtained as

$$C_h = \frac{2\beta^2 D^2 e^{\beta D}}{(e^{\beta D} + 2)^2}, \tag{40}$$

and near the critical point it can be expanded as

$$C_h = (\beta_c - 1)\, D_c^2 + O(t). \tag{41}$$

Hence, from Eqs. (39) and (41), the product

$$R_m\, C_h\, t^2 = -\tfrac{1}{2} \tag{42}$$

is what one would get by putting in mean-field values of exponents in Eq. (35), namely, $(\alpha, \widetilde{\beta}, \gamma, \delta) = (0, 1/2, 1, 3)$. This establishes the appropriateness of the scalar curvature R_m in encoding the zero-field critical behavior in the BEG model and further strengthens the association of R_m with the correlation volume of fluctuations in m, at least in the critical region. To complete the picture we also present the scaling behavior of R_m with the magnetic field H in the D plane, along the $t = 0$ line. It works out to

$$R_m \sim h^{-4/3} \quad (t = 0,\ \text{critical point}). \tag{43}$$

We turn now to the case of nonzero coupling between the quadrupole moments, namely, the full BEG case. The algebraic expressions involved are too lengthy, so we resort to numerical investigations for fixed values of the ratio $K/J = \omega$ and the neighborhood of a fixed critical point. With a nonzero ω the zero-field quadrupole moment in the normal phase is now obtainable via an implicit relation,

$$q = \frac{2e^{\beta q\omega - \beta D}}{2e^{\beta q\omega - \beta D} + 1}. \tag{44}$$

Near the critical point in the normal phase this implicit equation can be used to express a small deviation of the quadrupole moment from its critical value in terms of the deviation of the temperature from its critical value. It can be checked that the dependence on temperature is linear. Finally, a series expansion in the normal phase of R_m and C_h in the vicinity of, for example, the critical point at $\beta_c = 2.239$, $D_c = 0.45$ with $\omega = 0.1$ is given as

$$R_m^{-1} = -0.3451\, t^2 + O(t)^3 \tag{45}$$

and

$$C_h = 0.2155 - 0.4848\, t + O(t)^2. \tag{46}$$

We note that while the scaling of R_m is correct, the product of amplitudes $R_m C_h t^2$ equals 0.62 and not the universal value of 1/2 as expected with mean-field exponents and as verified in the case of the BC limit in the preceding. Nevertheless the product is always found to be greater than half and less than unity. For example, for the critical point at $\beta_c = 2.3932$, $D_c = 0.47$ with $\omega = 0.1$ the product equals 0.756, and for $\beta_c = 2.0126$, $D_c = 0.45$ with $\omega = 0.2$ the product equals 0.537. Thus it is seen that while the product has a weak dependence on the ratio ω and on the location of the critical point, it still remains small everywhere. We defer further analysis to a future investigation.

We now briefly discuss some general features of this geometry for the zero-field case. In Fig. 4(a) we obtain a semilog plot of the scalar curvature R_m vs β across the critical line at $D = 0.4$. R_m is seen to diverge to negative infinity from both the normal and superfluid phases. Further extending the semilog plot of R_m into the superfluid phase we see in Fig. 4(b) that after dropping to low values sufficiently far away from the critical line the curvature R_m begins a slower climb to negative infinity on approaching the zero temperature. In Fig. 4(c) the magnetization fluctuation σ_m^2 is seen to diverge at the critical point from either side and, it can be established, decays to 2/3 as $\beta \to 0$ and to zero as $\beta \to \infty$ in the superfluid phase, irrespective of D.

In conclusion, we observe an excellent scaling behavior of R_m and a very good agreement in the trends of R_m and σ_m^2 away from the critical point, especially in the normal phase. We are unable to account for the weak divergence of R_m towards zero temperature in the superfluid phase.

2. The q geometry

As mentioned earlier the q geometry becomes degenerate in the zero-field normal phase as can be seen by evaluating the determinant of the q metric, which is found to be zero in the normal phase. It would be worthwhile exploring the nature of the quadrupole fluctuations σ_q^2 in both the normal and the superfluid phases. In Fig. 5(a) we plot σ_q^2 vs β in the BC limit for $D = 0.4$ (the same as Fig. 4). Clearly, the quadrupole fluctuations in the normal phase are small but also quite flat in that the σ_q^2 values change very little all the way to $\beta = 0$ ($T \to \infty$) in which limit $\sigma_q^2 \to 2/9$ irrespective of D. In addition, we observe that σ_q^2 undergoes a discontinuous, finite jump at the critical point. We also note that the value of σ_q^2 at the critical boundary on the superfluid side is still small, which is consistent with the fact that zero-field criticality

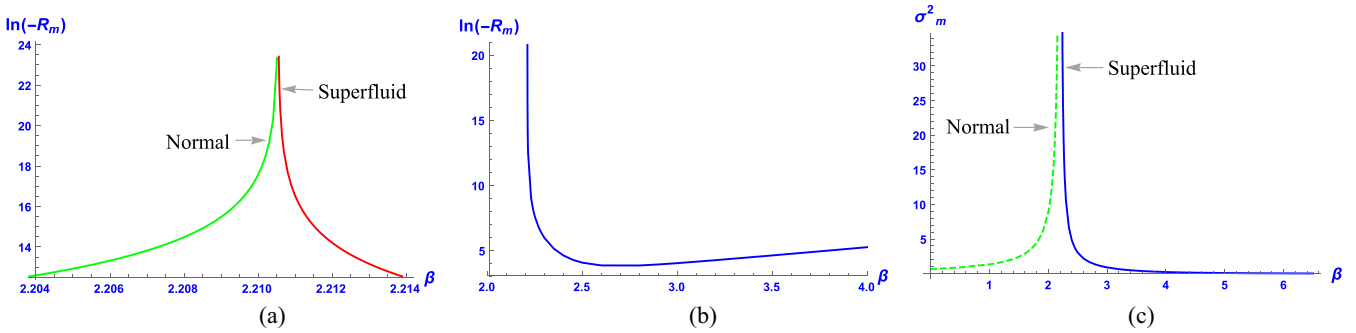

FIG. 4. (a) Plot of $\log(-R_m)$ vs β for the normal and superfluid (or ferromagnetic) phases, in the BC limit $\omega = 0$. (b) $\log(-R_m)$ vs β for the superfluid phase with β ranging from the critical value to higher values (lower temperatures). (c) Plot of the magnetization fluctuation σ_m^2 vs β. In all panels the value of $D = 0.4$, and the critical point is at $\beta = 2.211$.

in the BEG model is powered by the spin-spin correlations only [3]. Nonetheless, the discontinuity in σ_q^2 brings out the effect of criticality on the quadrupole-quadrupole interactions, which appear to be very different in the two phases. The superfluid scalar curvature R_q faithfully reflects the trend in the superfluid q-q interactions near criticality. In Figs. 5(b) and 5(c) we plot *along* the critical line, in turn, σ_q^2 and the superfluid curvature R_q vs D. Both quantities have been plotted at a fixed relative distance $t = (\beta - \beta_c)/\beta = 10^{-5}$ from the critical boundary of Fig. 2(a). It is seen that in the vicinity of the critical boundary within the superfluid phase the q curvature R_q and the quadrupole fluctuation σ_q^2 both remain small, especially for values of D away from the tricritical point at $D_{\rm tcr} = 0.462$, thereby underscoring the fact that the correlation length for the order parameter q remains small near criticality so that it does not play any direct role in phase ordering here. Near the tricritical point, however, to which we turn now, the case is not the same.

C. Geometry near the tricritical point

The tricritical point is the culmination of the triple line so that at this point three phases become one, and in the zero-field plane it joins the critical line and the coexistence line; see Fig. 2. The scaling laws at the tricritical point are different from the critical points, even for the mean-field case [9,24]. For the critical exponent β, while along the rest of the critical line we have $m \sim t^{1/2}$, on approaching the tricritical point we get $m \sim t^{1/4}$. Similarly, for the critical exponent δ, we have $m \sim H^{\frac{1}{3}}$ for ordinary critical points and $m \sim H^{\frac{1}{5}}$ for the tricritical point as can be quickly ascertained for the BC case from Eq. (13) and Eq. (14). Interestingly, the scaling exponents at the tricritical point equal their mean-field values for dimensions $d = 3$ as opposed to the upper critical dimension $d = 4$ for ordinary critical points. This can be seen from the formula for the upper critical dimension obtained from the Ginzburg criterion [24],

$$d_u = 2(\beta/\nu + 1).$$

The zero-field superfluid scalar curvature R_m, however, continues to diverge at the same rate

$$R_m \sim t^{-2}$$

as elsewhere on the critical line so that, in itself, it does not signal anything special happening to the m-m correlations at that point. However, as is apparent from Fig. 5(c) the q geometry already senses the vicinity of the tricritical point, with the scalar curvature R_q growing in magnitude for D values close to its tricritical value. This is also true of σ_q^2 in Fig. 5(b). At the tricritical point the superfluid q curvature diverges as

$$R_q \sim t^{-1}$$

with the quadratic fluctuation diverging as $\sigma_q^2 \sim t^{-1/2}$. We therefore conclude that the q-q correlations become more and

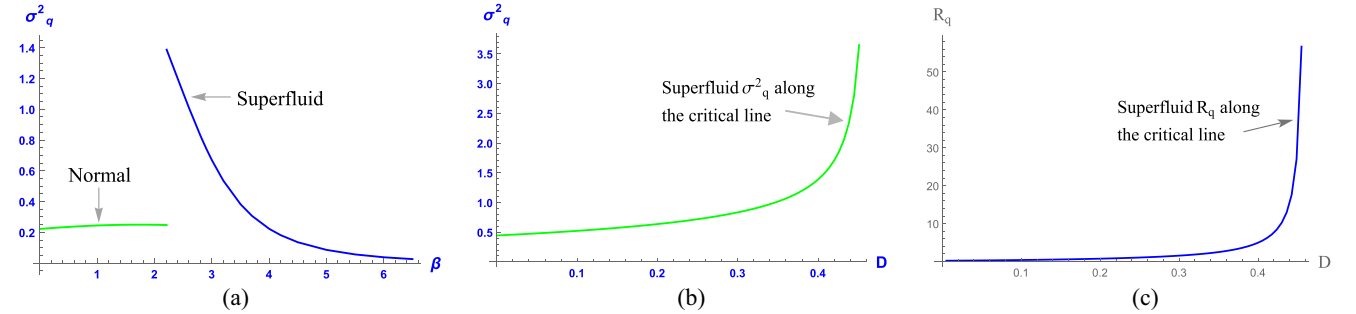

FIG. 5. (a) Plot of quadrupole fluctuation σ_q^2 vs β for $D = 0.4$ in both the normal and the superfluid phases. Notice the discontinuity at the critical point $\beta = 2.211$. Plots along the zero-field critical line of (b) superfluid quadrupole fluctuation σ_q^2 vs D and (c) of superfluid scalar curvature R_q vs D. Refer to Fig. 2(a) for the zero-field critical line. For (b) and (c) all points are at the reduced temperature inverse $t = 10^{-5}$. In all panels $\omega = 0$.

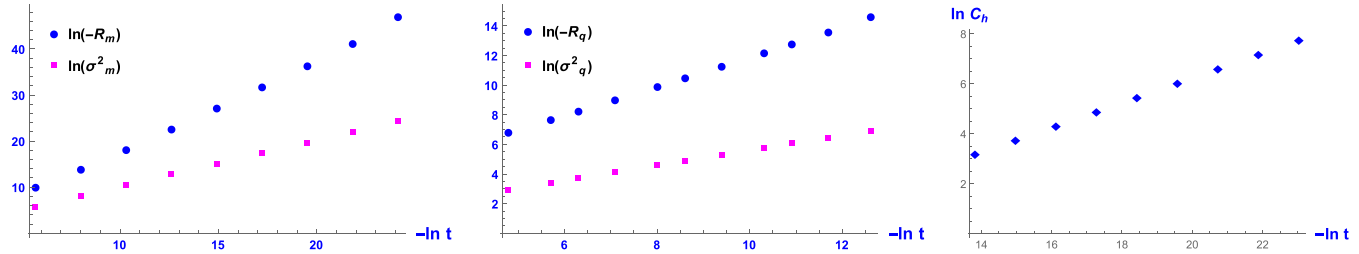

FIG. 6. (a), (b) The scaling behavior in the superfluid phase near the tricritical point at $D = 0.4621$, $\beta = 3$ for the BC limit ($\omega = 0$). (a) From the log-log plot of R_m and σ_m^2 vs t the slope is seen to be 2 and 1, respectively. (b) The slope from the log-log plot of R_q and σ_q^2 vs t is seen to be 1 and 1/2. (c) The slope of the log of the superfluid heat capacity C_h is 1/2, while in the normal phase C_h remains finite (not shown).

more long range as we approach the tricritical point, with ξ_q eventually diverging there. We establish the scaling behavior of the scalar curvatures in the superfluid phase graphically from Figs. 6(a) and 6(b). Figure 6(a) presents the log-log plot of R_m and σ_m^2 vs the reduced inverse temperature t. It is easy to establish the scaling behavior stated above from the log-log plot. Similarly, the log-log plot in Fig. 6(b) establishes the scaling behavior of R_q and σ_q^2.

Given that the upper critical dimension for the tricritical point is three, one would have expected the scaling of the scalar curvature to be 3/2 so that in three dimensions it would have led to $\nu = 1/2$ as expected. This is also suggested by the scaling of the heat capacity C_h near the tricritical point, which goes as

$$C_h \sim t^{-1/2}$$

in the superfluid phase as shown in Fig. 6(c). Therefore, from the exponent relation

$$\nu d = 2 - \alpha$$

the scalar curvature ought to scale as $t^{-3/2}$. Curiously, while neither R_m nor R_q has this scaling, it is the average of the two that turns out to be 3/2. Indeed, this could well be nothing more than a numerical fluke, and we suspect that a three-dimensional scalar curvature could possibly have been more apt to probe the tricritical point. We defer further investigation to the future.

In any case the geometry does inform us that microscopically the tricritical point is different from the rest of the zero-field critical line in that here both the q-q and the m-m correlations play a role in the phase transition.

Finally, as in Eq. (43) for the critical case, we obtain the tricritical scaling of R_m in the D plane along the $t = 0$ line. It is found to be

$$R_m \sim h^{-8/5} \quad (t = 0,\ \text{tricritical point}). \tag{47}$$

This is different from the critical value. While the $t = 0$ path is uncommon as a measure of scaling behavior for the correlation length, we do hope that it should be possible to check these with Monte Carlo simulations or finite-size scaling studies.

D. Geometry near the wing critical line

Here we shall restrict the non-zero-field investigations to the BC case. The geometric analysis can easily be extended to nonzero ω values, though we shall not pursue it here.

The critical line in the non-zero-field borders the wing coexistence region as mentioned previously in our description of the phase structure around Fig. 3. The intersection of the wing surface with the constant D plane (for $D > (\log 4)/3$) appears much like the T-P coexistence line of simple fluids, with the pressure field replaced by the H field and its conjugate density replaced by the magnetic moment. In Fig. 7(a) we plot a wing coexistence curve in the T-H plane for the BC case. It separates two paramagnetic phases labeled "A" and "B" and terminates at a critical point, much like in a van der Waals fluid. We obtain two different scaling behaviors by approaching the critical point from separate directions. In Fig. 7(b)

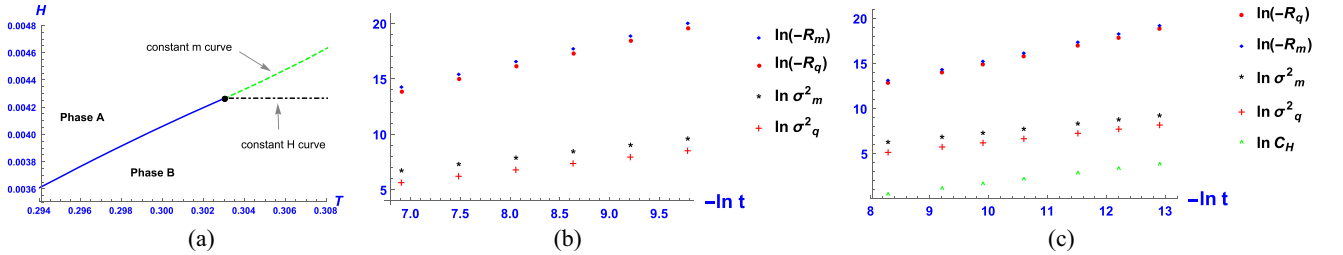

FIG. 7. (a) The BC wing coexistence curve in the T-H plane terminating with the (thick dot) critical point at $D_{cr} = 0.474$, $H_{cr} = 0.004$, $\beta_{cr} = 3.3$, and $m_{cr} = 0.301$. The coexisting phases are labeled A and B. Two directions of approach from the single phase region to the critical point are shown, one at constant $H = H_{cr}$ and the other at constant $m = m_{cr}$. Log-log plots in (b) and (c) show the scaling behavior in the D plane along, respectively, the constant m curve and the constant H curve. The slopes of R_m and R_q equal 2 in (b) and 4/3 in (c), while those of σ_m^2 and σ_q^2 equal 1 in (b) and 2/3 in (c). Also shown in (c) is a log-log plot of C_h with a slope of 2/3.

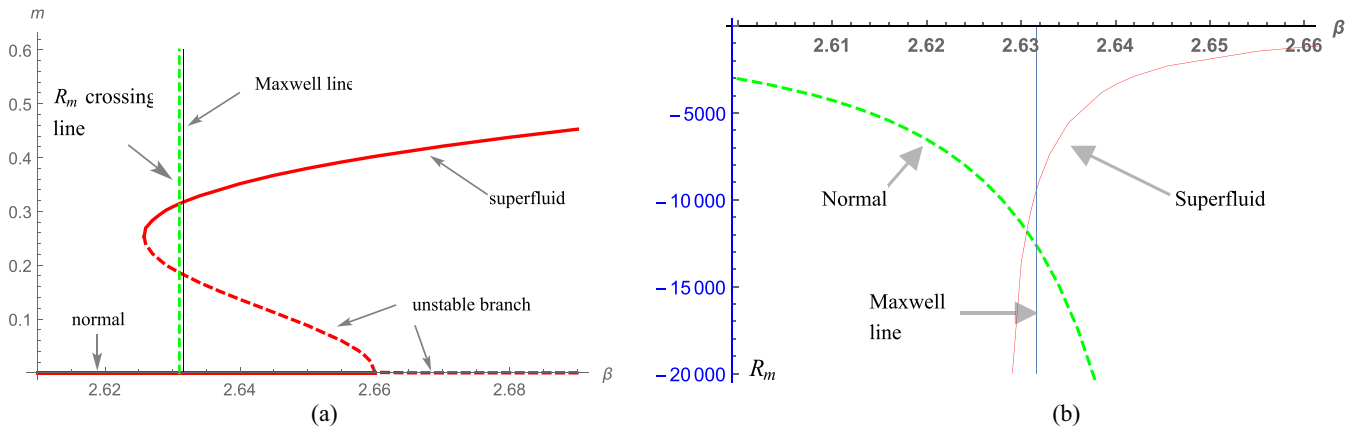

FIG. 8. Plots comparing R_m crossing to the free energy crossing (referred to as the Maxwell line). Both plots refer to the same first-order phase transition in zero field with $D = 0.511$ and at $\omega = 0.16$. In (a) the magnetization is plotted vs the inverse temperature β. The free energies of the normal and the superfluid phase become equal at the "Maxwell" line $\beta = 2.6316$, while the curvatures R_m in the two phases become equal at the R_m-crossing line at $\beta = 2.6305$. In (b) the curvature R_m for both the phases is plotted and is shown to cross near the Maxwell line at the aforementioned values of β. At the tricritical point for $\omega = 0.16$ the parameter values are $D = 0.5044,\ \beta = 2.515$.

we obtain log-log plots of R_m, R_q and the fluctuations σ_m^2, σ_q^2 along the constant m curve, with the magnetization fixed at its critical value. This is the standard path to ascertain critical exponents from the single phase region [7]. Here we see that $R_m \sim t^{-2}$. Interestingly, R_q also scales in exactly the same manner, thus suggesting that in non-zero-field region there is only one correlation length. This is known to be true in the one-dimensional spin one model [6] and was also confirmed geometrically in paper I. Meanwhile the heat capacity C_m remains finite near the critical point so that along the constant m path the exponent $\alpha = 0$, thus conforming to exponent relation $\nu d = 2 - \alpha$. We have also checked numerically that curvature R_m and the heat capacity C_m at the wing critical point conform to Eq. (42),

$$R_m C_m t^2 = -\tfrac{1}{2}, \tag{48}$$

which is identical to the case of the van der Waals fluid [18]. In Fig. 7(c) we show the scaling of R_q, σ_q^2, and C_h along the line $H = H_{cr}$. The heat capacity C_h here is analogous to C_p for fluids. It can be seen that along the constant H line

$$R_m \sim t^{-4/3}$$

and

$$C_h \sim t^{-2/3},$$

which again conforms to the exponent relation $\nu d = 2 - \alpha$. The amplitude relation of Eq. (42) is not followed, however. We notice from Fig. 7(c) that once again the curvatures R_m and R_q both have the same scaling.

V. GEOMETRY OF COEXISTENCE

In addition to encoding critical behavior, thermodynamic geometry is also known to efficiently probe phase coexistence and first-order phase transition. This was first discussed in [23] in the context of simple fluids. Following Widom's argument [21] equating correlation lengths in coexisting phases near criticality to the interface thickness, it was shown [23] by extensively using the NIST database for simple fluids that there was an excellent match between the numerically obtained scalar curvatures in the coexisting liquid and vapor phases near the critical point. It was also shown that for a reasonable distance from the critical point the scalar curvature obtained explicitly from the mean-field van der Waals model could predict the coexistence curve, thus nicely complementing the Maxwell construction. In the geometric context the coexistence point was obtained by locating the point of intersection of the scalar curvatures and hence (via the Ruppeiner conjecture) the correlation lengths of the two phases. This method of constructing the coexistence curve has since come to be known as the R-crossing method [25–27]. The geometric method advanced in [23] was quickly confirmed by numerical studies based on equations of state for the Lennard-Jones fluids [25]. The authors had found striking agreement between the phase envelope obtained by the R-crossing method and the one obtained from simulation data. In addition to phase coexistence the geometric investigations have also been fruitful in predicting the Widom line for the supercritical phase [23,25], though we will not be pursuing it here. Thermodynamic geometry of phase coexistence has also been investigated in magnetic systems [16] and black hole thermodynamic systems [28,29] among others.

In this section we geometrically investigate the phase coexistence regions in the zero-field region as well as the across the wings.

A. Zero-field coexistence between the normal and the superfluid phases

In Fig. 8(a) we plot the magnetization m vs the inverse temperature β in zero field at $D = 0.511$ and $\omega = 0.16$. For high temperatures (small β) only the normal phase with $m = 0$ exists. On lowering the temperature a metastable superfluid state ($m \neq 0$) begins to coexist with the globally stable (lower free energy) normal phase. On further lowering the temperature beyond the "Maxwell line" the superfluid state achieves global stability with its free energy "crossing" below that of the normal phase which is now metastable. This marks the

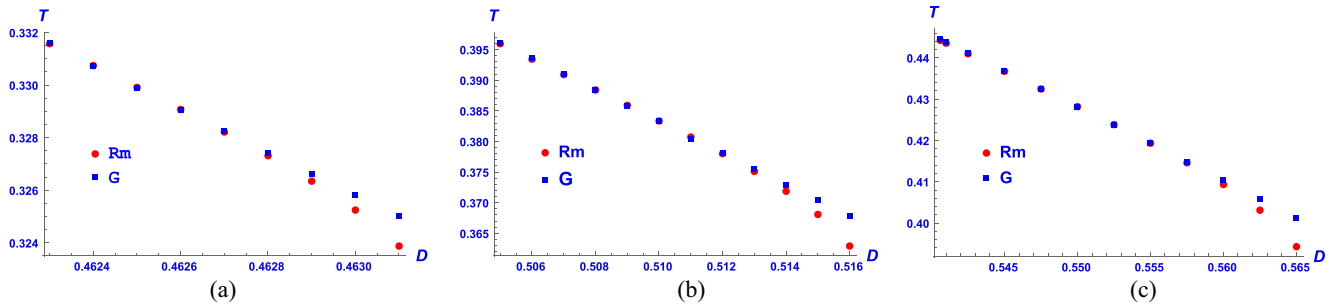

FIG. 9. Free energy crossing points labeled G and the scalar curvature R_m crossing points labeled R_m in the D-T plane for different values of ω. In each case the plots begin at the tricritical point. The BC limit for which $\omega = 0$ and the tricritical point is at $D = 0.4621,\ T = 1/3$. (b) $\omega = 0.16$ and the tricritical point is at $D = 0.5044,\ T = 0.397$. (c) $\omega = 0.30$, and the tricritical point is at $D = 0.5405,\ T = 0.445$.

first-order phase transition point as governed by free energy crossing. On further lowering the temperature the normal phase disappears, and the only stable (local as well as global) phase is the superfluid phase. Close to the Maxwell line is a dashed curve labeled the "R_m crossing line" which indicates the temperature at which the m curvatures of the coexisting phases cross each other. This is further elaborated in the curvature R_m vs β plot in Fig. 8(b), in which the curvatures R_m of the normal and the superfluid phases are seen to cross each other at a temperature close to the free energy crossing temperature indicated by a vertical line.

The first-order phase transition in zero field is understood as a phase separation between the normal and superfluid phases in the context of the BEG model and between the magnetic and the impurity dominated nonmagnetic phases in the BC case. In the BC case and also for small quadrupole-quadrupole coupling (ω small) in the BEG case the phase separation is governed by superfluid ordering via the order parameter m. Thus for $D > D_{\rm tcr}$ the only way to sustain a superfluid order in the helium mixture (or a magnetic order) is to separate into two phases with He^3 atoms (or nonmagnetic impurities) dominating the normal phase. For larger values ω the nonmagnetic intermolecular interaction force between molecules begins to play an increasingly important role in phase separation, [3]. Unfortunately, we shall not be able to examine this trend geometrically since, with the q geometry defined only in the superfluid phase, the q curvature in the normal phase will not be available for comparison.

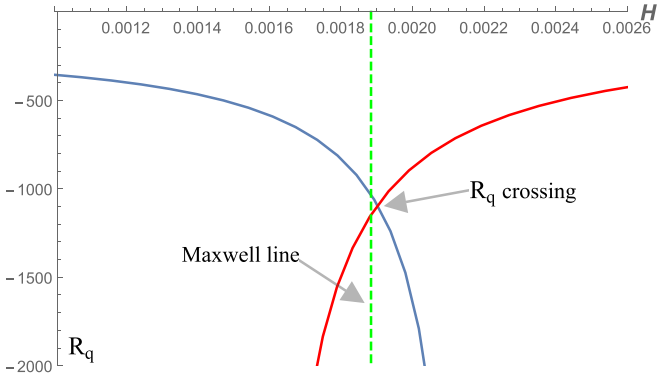

FIG. 10. R_q crossing diagram across the wing for the BC case ($\omega = 0$). Plot of R_q vs H in coexisting phases across the wing region at $D = 0.47$ and $\beta = 3.3$.

In each of Figs. 9(a), 9(b), and 9(c), respectively, for $\omega = 0,\ 0.16,\ 0.3$ we plot in the D-T plane two coexistence curves, the standard one predicted by the free energy crossing, labeled by points "G," and the one predicted by the R-crossing method, with points labeled by "R_m." Each of the plots starts from the tricritical point for its ω value. Remarkably enough, up to a reasonable distance from the tricritical point there is an excellent agreement in the coexistence curves predicted by the free energy and by the curvature crossings. We also notice that as we tune up the quadrupolar interaction by increasing ω, the range of temperatures for which the coexistence curves agree increases. This could probably have to do with the observation in [3] that increasing the intermolecular interaction strength (quadrupolar coupling in the Hamiltonian) positively induces phase separation, which at $\omega = 0$ is controlled solely by the spin-spin interactions. Lack of a nontrivial q geometry in the normal phase limits our analysis in this case.

B. Coexistence across the wing region

We compare both the q curvature and the m curvature for coexisting phases across the wings. We restrict ourselves to the BC case for simplicity, though the qualitative picture remains the same for small values of ω. We shall be plotting the coexistence curves between the two paramagnetic phases [refer to Fig. 7(a) showing two coexisting paramagnetic phases labeled "A" and "B"] in the T-H plane as predicted by the free energy crossing, the R_m crossing, and the R_q crossing. Interestingly, it turns out, it is the q geometry whose coexistence curve prediction matches better the standard coexistence curve obtained via free energy crossing.

In Fig. 10 we plot R_q vs H for coexisting paramagnetic phases across the wing in the BC model. R_q crossing is seen to be close to the free energy crossing. Further, in Fig. 11 we plot the coexistence curves generated by the self-crossings of the free energy G, of R_m and of R_q. While the R_q generated coexistence curve is quite close to the standard free energy coexistence curve, the R_m curve seems to diverge quickly. This could probably be an indication that the quadrupolar correlations play an important role in phase separation across the wing. Of course, any such statement must be supported by further analysis, which we defer to a future investigation.

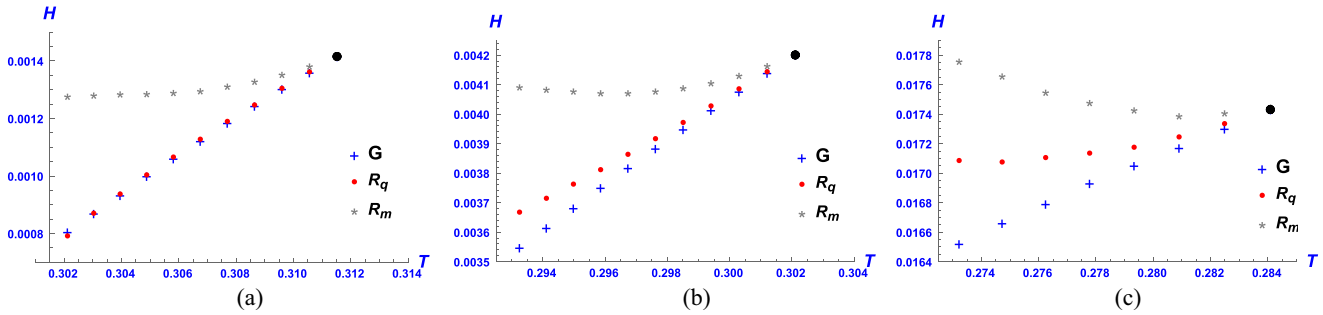

FIG. 11. The free energy crossing points labeled G and the curvature crossing points labeled R_q and R_m in the H-T plane for (a) $D = 0.4681$ and $\beta_{\text{critical}} = 3.2$, (b) $D = 0.47413$ and $\beta_{\text{critical}} = 3.3$, and (c) $D = 0.495105$ and $\beta_{\text{critical}} = 3.5$. The free energy crossing points lie on the coexistence "wing" B' of Fig. 1.

We also note from Fig. 11 that for wing regions closer to the triple line the coincidence between the R_q and the free energy coexistence curves persists for a longer distance from the wing critical point. In Fig. 12 we plot the equilibrium free energy G vs H for different distances from a wing critical point. The reference figure for these is Fig. 11(b). The free energy self-crossing is compared to the R_q crossing in each subfigure.

The discussions around Figs. 9 and 11 suggest that the triple line and the tricritical point at its terminus play a strong role in organizing the thermodynamic behavior around their vicinity. At least the geometry does carry the signature of the triple line in a deep neighborhood of it.

VI. CONCLUSIONS

Formally, this paper is a continuation to the mean-field case of the thermodynamic geometric investigation of spin one model started in paper I where the one-dimensional spin one chain was analyzed. Thematically, however, there is a qualitative difference in the two. In contrast to paper I where the role of geometry was mainly to *confirm* that the curvatures are proportional to the exactly calculable correlation length(s), in this work geometry is called upon to play a stronger role in that it *predicts* a correlation length for the mean-field model, which otherwise contains no direct information on correlations.

We have constructed two complementary geometries which are demonstrably responsive in turn to the correlations in the magnetization and the quadrupolar order parameters. Significantly, the scalar curvatures are shown to conform to the two-scale factor universality relation between the heat capacity and the correlation volume [20], and the geometric correlation length is shown to have a superior scaling behavior compared to the Ginzburg-Landau correlation length. The tricritical point is also investigated, and, while the geometry there correctly identifies the role of both the spin and the quadrupole fluctuations, the curvatures there do not scale as expected.

Geometric coexistence curves are plotted in the zero- and non-zero-field regions, and they are found to agree remarkably well with the standard coexistence curves obtained via the Maxwell construction. In addition, geometry is also seen to respond to the relative importance of the two order parameters in ordering the phase dynamics in different regimes. Thus, while the magnetization correlations seem to drive

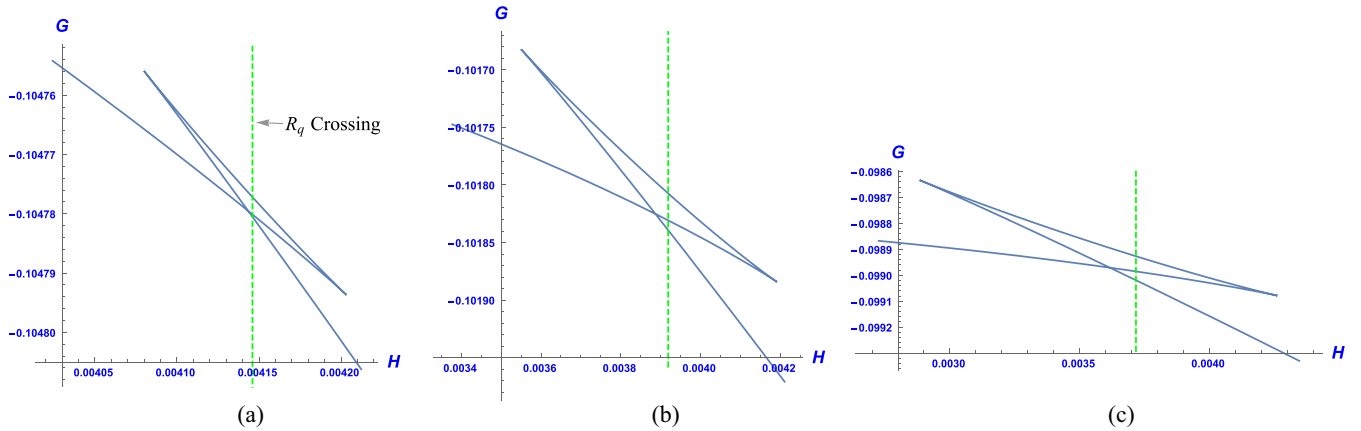

FIG. 12. Plots of isotherms of free energy in the G-H plane at $D = 0.47413$. While the free energy crossing gives the phase transition point via the Maxwell construction, the green dashed line represents the R_q crossing point. At the critical point $\beta_{\text{critical}} = 3.3$. The parameters here are the same as in Fig. 11(b). (a) $\beta = 3.32$, the free energy G crosses at $H = 0.004144$, while R_q crosses at $H = 0.004146$ with a relative separation of 1.62%, (b) $\beta = 3.36$ and the G and R_q crossings are at $H = 0.003888$ and 0.003919 with separation of 4.84%, and (c) $\beta = 3.4$ with G and R_q crossings at $H = 0.003619$ and 0.003717, respectively, with a relative separation of 7.11%. The values of R_q at the R_q crossing are, respectively, -8618, -1345, and -644.

phase separation in zero field, it is the quadrupole correlations which appear to drive phase separation in nonzero field.

Similar to [23] where the geometric investigation of phase coexistence was first initiated in the context of pure fluids this work probes phase coexistence in model ferromagnetic systems. To the best of our knowledge this is the first such comprehensive work, with similar themes having appeared previously in a limited sense in [16,17]. On the other hand, an accurate geometric construction of the coexistence curves should also be seen as a confirmation of the curvature-correlation correspondence in the noncritical regions (i.e., the *weak* Ruppeiner conjecture).

Our analysis strongly suggests that thermodynamic geometry provides valid correlation length estimates for the mean-field models in both critical and noncritical regimes. We sincerely hope that our studies will motivate a geometry based analysis of multicritical phenomena and spin models with multiple order parameters. Further, it would be good to test and complement the results of our analysis with Monte Carlo simulations, finite-size scaling studies, and renormalization group analysis.

ACKNOWLEDGMENTS

We thank George Ruppeiner for discussions and his extensive comments on an advanced draft of paper I which also helped refine some of our analysis in this paper. A.S. thanks Ritu Sharma for useful discussions. This work was supported by the Department of Science and Technology (DST), New Delhi, India, under the grant (File number MTR/2017/001001).

[1] R. Sanwari and A. Sahay, Phys. Rev. E **105**, 034134 (2022).
[2] G. Ruppeiner, Phys. Lett. A **383**, 703 (2019).
[3] M. Blume, V. J. Emery, and R. B. Griffiths, Phys. Rev. A **4**, 1071 (1971).
[4] M. Blume, Phys. Rev. **141**, 517 (1966).
[5] H. W. Capel, Physica **32**, 966 (1966).
[6] S. Krinsky and D. Furman, Phys. Rev. B **11**, 2602 (1975).
[7] R. K. Pathria and P. D. Beale, *Statistical Mechanics*, 3rd ed. (Butterworth Heinemann, Oxford, 2011).
[8] D. Mukamel and M. Blume, Phys. Rev. A **10**, 610 (1974).
[9] P. M. Chaikin and T. C. Lubensky, *Principles of Condensed Matter Physics* (Cambridge University Press, Cambridge, 1995).
[10] J. Strečka and M. Jaščur, Acta Phys. Slovaca **65**, 235 (2015).
[11] W. Hoston and A. N. Berker, Phys. Rev. Lett. **67**, 1027 (1991).
[12] Y. L. Wang and K. Rauchwarger, Phys. Lett. A **59**, 73 (1976).
[13] R. B. Griffiths, Physica **33**, 689 (1967).
[14] A. K. Jain and D. P. Landau, Phys. Rev. B **22**, 445 (1980).
[15] H. Janyszek and R. Mrugala, Phys. Rev. A **39**, 6515 (1989).
[16] A. Dey, P. Roy, and T. Sarkar, Physica A **392**, 6341 (2013).
[17] R. Erdem and N. Alata, Eur. Phys. J. Plus **135**, 911 (2020).
[18] G. Ruppeiner, Rev. Mod. Phys. **67**, 605 (1995); **68**, 313 (1996).
[20] D. Stauffer, M. Ferer, and M. Wortis, Phys. Rev. Lett. **29**, 345 (1972).
[21] B. Widom, Physica **73**, 107 (1974).
[22] R. Maity, S. Mahapatra, and T. Sarkar, Phys. Rev. E **92**, 052101 (2015).
[23] G. Ruppeiner, A. Sahay, T. Sarkar, and G. Sengupta, Phys. Rev. E **86**, 052103 (2012).
[24] I. D. Lawrie and S. Sarbach, Theory of tricritical points, in *Phase Transitions and Critical Phenomena*, Vol. 9, edited by C. Domb and J. L. Lebowitz (Academic Press, London, 1984).
[25] H. O. May and P. Mausbach, Phys. Rev. E **85**, 031201 (2012).
[26] J. Jaramillo-Gutiérrez, J. L. López, and J. Torres-Arenas, J. Mol. Liq. **295**, 111625 (2019).
[27] G. Ruppeiner, P. Mausbach, and H. May, Phys. Lett. A **379**, 646 (2015).
[28] A. Sahay and R. Jha, Phys. Rev. D **96**, 126017 (2017).
[29] P. Chaturvedi, S. Mondal, and G. Sengupta, Phys. Rev. D **98**, 086016 (2018).